

## Valence state of iron and molybdenum cations under conditions of anionic deficiency in $\text{Sr}_2\text{FeMoO}_{6-\delta}$

*Nikolay Kalanda, Marta Yarmolich, Dong-Hyun Kim, Dalis Baltrūnas, Kestutis Mažeika, Sigitas Tamulevičius, Mindaugas Andrulevičius, Nikolai A. Sobolev\**

Dr. N.A. Kalanda, Dr. M.V. Yarmolich  
Scientific-Practical Materials Research Centre of the NAS of Belarus, P. Brovka St. 19, 220072 Minsk, Belarus

Prof. D.-H. Kim  
Department of Physics, Chungbuk National University, 1 Chungdaero, Seowongu, Cheongju 28644, South Korea

Dr. D. Baltrūnas, Dr. K. Mažeika  
Center for Physical Sciences and Technology, Savanorių ave. 231, LT-02300 Vilnius, Lithuania

Prof. S. Tamulevičius, Dr. M. Andrulevičius  
Institute of Materials Science of Kaunas University of Technology, Baršausko St. 59, LT-51423 Kaunas, Lithuania

Prof. N.A. Sobolev\*  
Departamento de Física and I3N, Universidade de Aveiro, 3810-193 Aveiro, Portugal,  
National University of Science and Technology MISiS, 119049 Moscow, Russia

\* Corresponding author. E-Mail: [sobolev@ua.pt](mailto:sobolev@ua.pt)

**Keywords:** strontium ferromolybdate; oxygen stoichiometry; defect formation; oxygen desorption

The activation energy of oxygen diffusion in strontium ferromolybdate  $\text{Sr}_2\text{FeMoO}_{6-\delta}$  was determined by the Merzhanov technique based on the temperature dependences of the oxygen desorption dynamics. It was found that the activation energy has a minimal value of 76.7 kJ/mol at  $\delta = 0.005$  and maximum value of 156.3 kJ/mol at  $\delta = 0.06$ . It was suggested that, with an increase in the oxygen vacancies concentration, an interaction occurs between them and the nearest cations with the subsequent formation of associates of various types that are less mobile than the single anion vacancies. According to the Mössbauer spectroscopy data, it was established that the appearance of oxygen vacancies and their ordering contribute to the isomer shift, and some of the iron ions occupy the tetrahedral (or close to it) positions in the lattice. This indicates the formation of associates of oxygen vacancies. The results of XPS studies have shown that the increase in the concentration of oxygen vacancies results in a decrease of the  $\text{Mo}^{6+}$  and  $\text{Fe}^{2+}$  concentration. At the same time, the number of  $\text{Mo}^{5+}$  and  $\text{Fe}^{3+}$  cations increases due to the redistribution of the electron density, and molybdenum cations in a different valence state ( $\text{Mo}^{4+}$ ) appear.

## 1. Introduction

Strontium ferromolybdate  $\text{Sr}_2\text{FeMoO}_{6-\delta}$  (SFMO) with the double perovskite structure has attracted much attention because of possible applications in magnetic field sensors and other spintronic devices due to its half-metallic characteristics with a 100% spin polarization, relatively high Curie temperature of 410 – 450°K and large values of the room-temperature magnetoresistance ( $\sim 3 - 10\%$ ) in magnetic fields below 1°T<sup>[1-3]</sup>. Moreover, the SFMO with its mixed oxygen-ion and electronic conductivity may be applied in gas sensors, as a cathode material in solid-fuel cells, membranes for the selective segregation of oxygen from gaseous mixtures, etc.<sup>[4-6]</sup>

Physical-chemical properties of the SFMO considerably depend on the oxygen stoichiometry which influences the degree of superstructural ordering of iron and molybdenum cations, the orbital, charge and spin degrees of freedom, and thus these properties particularly depend on the electronic exchange interaction between  $\text{Fe}^{3+}$  and  $\text{Mo}^{5+}$ <sup>[7-10]</sup>. The crystal lattice distortions, caused by the deficiency in the anion sublattice, influence the bond lengths and spatial placement of the  $\text{Fe}^{3+}-\text{O}^{2-}-\text{Mo}^{5+}$  chains, significantly changing the value of the exchange interaction integral, depending both on the electronic orbitals overlap and on the bond angles between them<sup>[11-13]</sup>. Moreover, the presence of oxygen ions and their vacancies on the SFMO grain surface promotes the change of the electron charge density at the intergrain boundaries and in the subsurface grain volume<sup>[14-16]</sup>. In this case, the charge density will be determined by the partial oxygen pressure in the surrounding gaseous medium during the synthesis and, correspondingly, it will modify the electrical transport properties of the compound, which will make it possible to use the SFMO as a resistive-type gas sensor. In this case, the efficiency of the sensor considerably depends on the concentration of oxygen defects and their mobility. The oxidation-reduction processes can reversibly change the oxygen stoichiometry both in the grains and grain boundaries, so that they can influence the magnetic and galvanomagnetic properties<sup>[17-19]</sup>. Therefore, a well-defined SFMO sample fabrication technology providing reproducible physical characteristics is required to obtain

samples with a controllable oxygen content, enabling further understanding of the underlying processes which determine the lifetime of devices based on SFMO.

It should be mentioned that the homogeneity range of  $\text{Sr}_2\text{FeMoO}_{6-\delta}$  in terms of the oxygen index is rather narrow, covering the interval from  $\delta = 0$  to  $\delta = 0.086$ . In this way, at an annealing temperature of 1473 K the oxygen partial pressure should not be higher than  $\log_{10}p(\text{O}_2) = -10.20$  or lower than  $\log_{10}p(\text{O}_2) = -13.70$  ( $p$  measured in Pa), as the decomposition of the double perovskite takes place at pressures outside this range. At partial pressures above the upper limit ( $\log_{10}p(\text{O}_2) \geq -10.20$ ),  $\text{Sr}_2\text{FeMoO}_{6-\delta}$  is decomposed according to the equation  $\text{Sr}_2\text{FeMoO}_6 + \frac{1}{2}\text{O}_2 = \text{SrMoO}_4 + \text{SrFeO}_3$ . In the case of partial pressures below the lower limit ( $\log_{10}p(\text{O}_2) \leq -13.70$ ), SFMO decomposes into simpler oxides followed by the formation of SrO, Fe and Mo. This circumstance imposes additional difficulties in obtaining a magnetic material with the required oxygen index. Taking into account the information stated above, the narrow homogeneity range of the compound and considerable influence of the intragranular oxygen, as well as of the surface oxygen, on the physical properties of the SFMO, there is a necessity of an investigation into the character of exchange processes between the complex oxide and the gaseous phase.

Unfortunately, possibilities of revealing modifications and distortions of the SFMO crystal structure, caused by the complexity of its composition, using classical methods of the structural phase analysis of nanoparticles are limited, thereby hindering detailed understanding of the structural properties on a nanometer scale. Thus, a detailed study of the local atomic ordering in magnetic SFMO grains is of special importance. It is expected that such studies will reveal the arrangement of atoms at distances on an interatomic scale, taking place due to the change in the oxygen vacancy concentration and superstructural ordering of the Fe/Mo cations. Thus, a number of authors, using the x-ray photoelectron spectroscopy (XPS), found that a mixed-valence state of the Fe and Mo cations is observed in SFMO, depending on the oxygen concentration and superstructural ordering degree of those cations. In this situation, the coexistence of both chain fragments,  $30\%(\text{Fe}^{3+}-\text{Mo}^{5+})$  and  $70\%(\text{Fe}^{2+}-\text{Mo}^{6+})$ , is possible [20–22].

It is known that the Mössbauer spectroscopy technique using the  $^{57}\text{Fe}$  isotope permits to obtain qualitative and quantitative information on the phase composition, specific properties of the electronic structure (density) and magnetic ordering of each phase, being based on a complex analysis of hyperfine parameters of local configurations of iron ions <sup>[20]</sup>.

Taking the charge neutrality into consideration, the oxygen deficiency can introduce additional  $\text{Fe}^{2+}$  into the compound and affect Mössbauer spectra parameters. Mössbauer spectroscopy studies have previously shown that the majority (> 61%) of Fe sites corresponding to the main sextet of the spectrum have a valence state of iron which is not pure  $\text{Fe}^{3+}$  but intermediate between  $\text{Fe}^{3+}$  and  $\text{Fe}^{2+}$  because of the presence of a delocalized Mo electron on Fe in the perfectly ordered SFMO <sup>[23–25]</sup>. Other components (sextets) at low temperatures represent iron sites differently affected by an imperfect Fe–Mo ordering or by other defects and are closer to the  $\text{Fe}^{3+}$  state according to the hyperfine field and center shift of Mössbauer spectra.

We report an investigation into the oxygen desorption in SFMO and a determination of the energy parameters of the anion mobility as a function of the defect concentration. Correlations between the oxygen non-stoichiometry and the formation of various anionic defects and their associates, superstructural ordering of the Fe/Mo cations and the valence state of iron are comprehensively studied by the Mössbauer spectroscopy.

## **2. Experimental**

Polycrystalline  $\text{Sr}_2\text{FeMoO}_{6-\delta}$  samples were synthesized from  $\text{SrFeO}_{3-x}$  and  $\text{SrMoO}_4$  precursors obtained by a conventional ceramic technology from the  $\text{MoO}_3$ ,  $\text{Fe}_2\text{O}_3$  oxides and the strontium carbonate  $\text{SrCO}_3$ . Grinding and stirring of the stoichiometric blends of initial reagents,  $\text{SrCO}_3 + 0.5\text{Fe}_2\text{O}_3$  and  $\text{SrCO}_3 + \text{MoO}_3$ , were carried out in a vibromill in alcohol for 3 hours. The obtained mixtures were dried at 350 K and pressed into pellets. After the synthesis of the  $\text{SrFeO}_{3-x}$  and  $\text{SrMoO}_4$  precursors, the initial annealing was carried out in air at 970 K and 1070 K for 20 and 40 hours, respectively. A secondary grinding was applied to increase the homogeneity of the

annealed mixtures. The final synthesis for obtaining the  $\text{SrFeO}_{3-x}$  single-phase compound was carried out at  $T = 1470$  K for 20 hours in a stream of argon, while the synthesis of the  $\text{SrMoO}_4$  single-phase compound was carried out at  $T = 1470$  K for 40 hours at  $p(\text{O}_2) = 0.21 \times 10^5$  Pa. The oxygen content in the  $\text{SrFeO}_{3-x}$  samples was determined by weighing them before and after their complete reduction in a stream of oxygen at 1370 K for 20 hours to a simple oxide SrO and metal Fe. As a result, the starting samples had the composition  $\text{SrFeO}_{2.52}$ . The pellets, pressed from a mixture of reagents  $\text{SrFeO}_{2.52} + \text{SrMoO}_4$ , with a diameter of 10 mm and a thickness of 4 – 5 mm, were annealed in a flow of the gas mixture 5% $\text{H}_2/\text{Ar}$  at 1420 K for 5 hours. As a result of the synthesis, pellets with the  $\text{Sr}_2\text{FeMoO}_{6-\delta}$  single-phase composition were obtained. The oxygen content in the  $\text{Sr}_2\text{FeMoO}_{6-\delta}$  samples was determined by weighing them before and after their complete reduction in a stream of oxygen at 1370 K for 20 hours to a simple oxide SrO and metals Fe and Mo. It has been determined that the starting samples had the composition  $\text{Sr}_2\text{FeMoO}_{5.99}$ .

The oxygen desorption from SFMO was studied using a Setaram Labsys TG–DSC16 measuring setup at various heating rates in a range from 300 – 1420 K. The samples were kept until the thermodynamic equilibrium with the gaseous medium was achieved, and then they were cooled down to RT in a flow of the 5% $\text{H}_2/\text{Ar}$  gas mixture. The evidence of the achievement of thermodynamic equilibrium was the absence of a change of the sample mass at a fixed sample temperature. The mass of the samples was controlled by weighing with an accuracy of  $\pm 3 \times 10^{-5}$  g.

The crystal lattice parameters and the degree of the superstructural ordering of cations ( $P$ ) were determined using the ICSD–PDF2 (Release 2000) database and POWDERCELL [26], FullProf [27] software by the Rietveld technique on the basis of XRD data obtained in a Philips X'Pert MPD diffractometer using the Cu- $K\alpha$  radiation at RT. XRD patterns were recorded at RT at a rate of 60 deg/h in the 10 – 90 deg angular range.

Mössbauer spectra were recorded using a  $^{57}\text{Co}(\text{Rh})$  source in the transmission geometry. The spectra were measured at approximately 10 K placing the samples in a closed-cycle He cryostat (Advanced Research Systems, Inc.). The Mössbauer spectra were fitted by several sextets applying

the WinNormos software. The isomer shift of Mössbauer subspectra is given in the text relatively to the metallic iron at RT.

For the XPS measurements a Thermo-Scientific ESCALAB 250Xi spectrometer (Thermo Fisher Scientific, UK) with a monochromatic Al-K $\alpha$  radiation ( $h\nu = 1486.6$  eV) as excitation source was used. The base pressure in the analytical chamber during analyses was kept below  $5 \times 10^{-7}$  Pa. The analyzed surface was 0.9 mm in diameter, while all spectra were acquired using a “take off” angle of 90 deg. The energy scale of the system was calibrated according to the Au-4f $_{7/2}$ , Ag-3d $_{5/2}$  and Cu-2p $_{3/2}$  peak positions. For the peak fitting procedure and atomic concentration calculations, the Thermo-Scientific Advantage software (v5.979) was used. All peaks were fitted using a sum of Lorentzian-Gaussian (30:70) functions for the analyzed elements.

## 2. Results and Discussion

The study of the processes of oxygen desorption in polycrystalline Sr $_2$ FeMoO $_{6-\delta}$  samples with the variation of the  $\delta$  parameter was carried out using the thermogravimetric analysis data obtained for different heating rates ( $v_h = 3, 5, 7, 9$  and  $11$  deg/min) in a continuous flow of the gas mixture 5%H $_2$ /Ar in the temperature range from 300 – 1420 K.

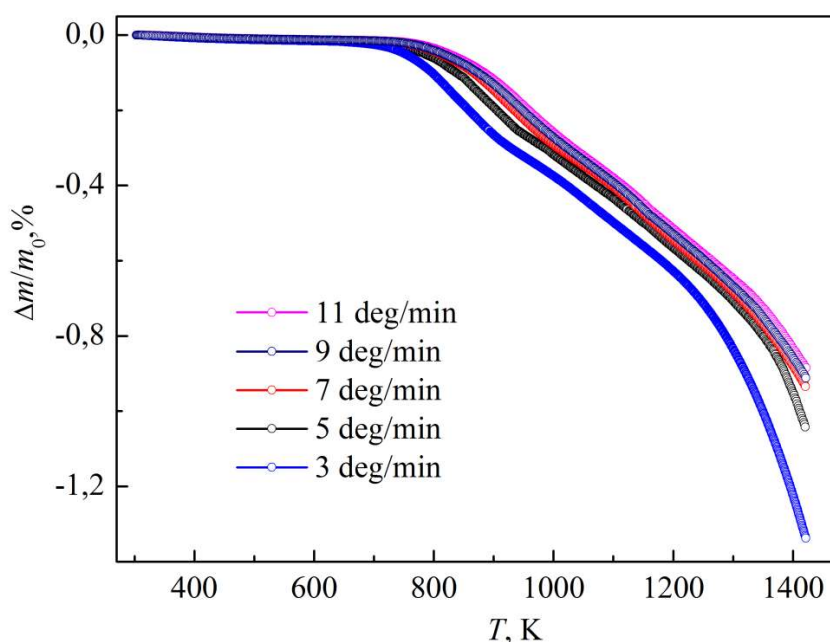


**Figure 1.** Temperature dependence of the mass change of SFMO samples at heating rates of 3, 5, 7, 9 and 11 deg/min.

**Figure 1** shows that the pronounced release of oxygen during sample heating at a rate of 3 deg/min starts at  $T \sim 713$  K. At  $T = 1420$  K the mass change ( $\Delta m/m_0$ ) of the sample achieves 1.34%. With the heating rate increasing to 11 deg/min, the temperature of the onset of oxygen emission shifts towards higher temperatures and reaches  $\sim 775$  K <sup>[28]</sup>, and at  $T = 1420$  K the value of  $\Delta m/m$  equals 0.88% <sup>[28]</sup>. This indicates the dependence of the oxygen desorption process on the concentration of anionic defects in the SFMO structure.

Based on the earlier calculations of the activation energy of the oxygen diffusion by the Merzhanov method, it was found that, at the initial stage of oxygen desorption from  $\text{Sr}_2\text{FeMoO}_{6-\delta}$ , the activation energy has a minimum value of  $E_a = 76.7$  kJ/mol at  $\delta = 0.005$  (inset in **Figure 2**) <sup>[28-31]</sup>. The  $\delta$  values were calculated by **Equation 1**:

$$\mu_{\text{Sr}_2\text{FeMoO}_{6-\delta}} = \frac{(m_0 - \Delta m)\mu_{\text{Sr}_2\text{FeMoO}_{5.99}}}{m_0}, \quad (1)$$

where  $m_0$  is the mass of the  $\text{Sr}_2\text{FeMoO}_{5.99}$  sample, and  $\mu_{\text{Sr}_2\text{FeMoO}_{5.99}}$  is its molar mass;  $(m_0 - \Delta m)$  is the mass of the  $\text{Sr}_2\text{FeMoO}_{6-\delta}$  sample, and  $\mu_{\text{Sr}_2\text{FeMoO}_{6-\delta}}$  its molar mass. With increasing concentration of oxygen vacancies,  $E_a$  reaches 156.3 kJ/mol at  $\delta = 0.06$  (inset in Figure 2).

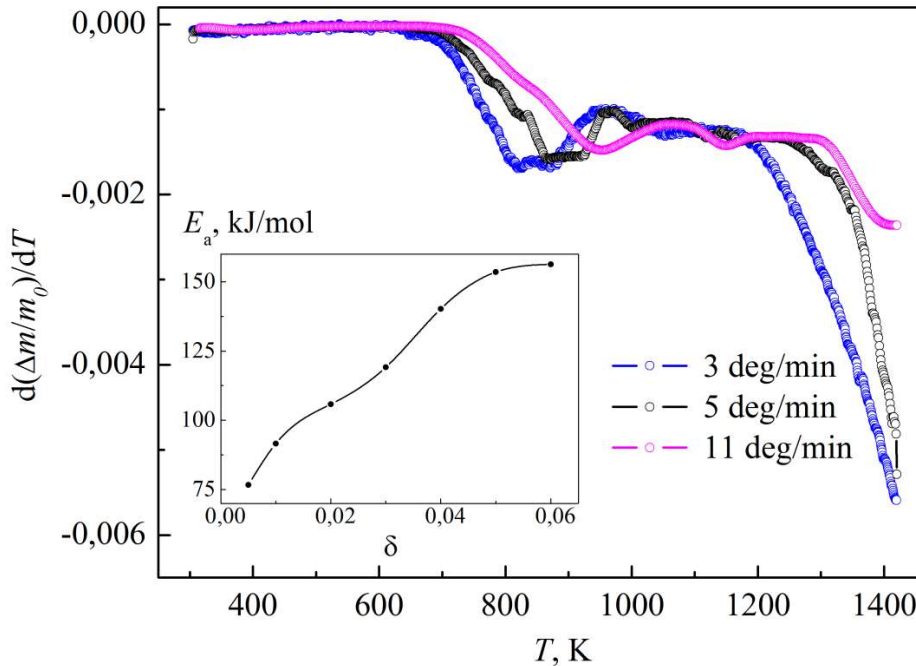


**Figure 2.** Temperature dependence of the rate of mass change of SFMO samples at heating rates of 3, 5 and 11 deg/min. The inset shows the dependence of the activation energy of oxygen diffusion  $E_a$  on the oxygen nonstoichiometry  $\delta$ .

The environment of oxygen in the SFMO compound plays an important role in the processes of its desorption. The first and most reactive form is oxygen adsorbed by the surface of the grains<sup>[32]</sup>. Therefore, due to the presence of a developed surface in polycrystalline samples, the rate of oxygen desorption processes in the temperature range from 700 – 1070 K is determined by the kinetics of the reaction at the gas-solid interface. At the same time, an increase in  $E_a$  with increasing  $\delta$  indicates a contribution to the desorption of oxygen also of the O1 and O2 anions which have different crystallographic positions, but almost the same binding energy (**Figure 3**).

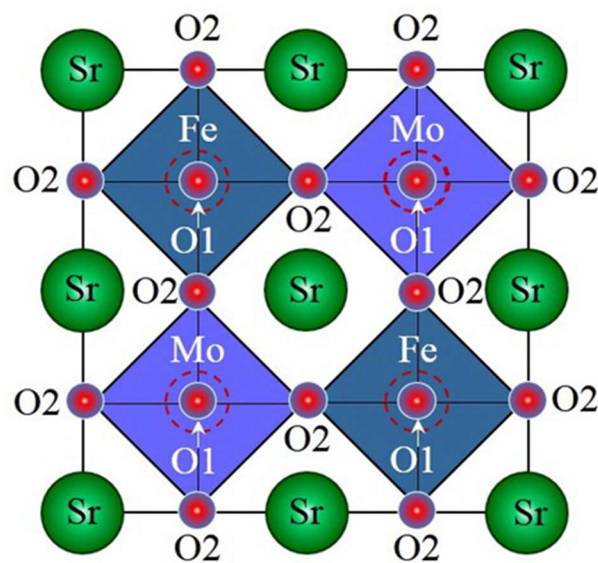


**Figure3** (color online). Schematic representation of the  $\text{Sr}_2\text{FeMoO}_{6-\delta}$  double perovskite unit cell projected on its base plane.

With the temperature increasing further above 1070 K and with simultaneously growing  $\delta$ , a significant increase in  $E_a$  was detected, which indicates the appearance of forces preventing the diffusion of oxygen during its desorption. It can be assumed that as  $\delta$  increases, the mechanism of defect formation changes, affecting the mobility of anions. It is quite possible that, with increasing concentration of oxygen vacancies, an interaction occurs between them and the nearest cations, with the subsequent formation of associates of various types that are less mobile than single anion vacancies. The latter ones and their associates are known to contribute to the redistribution of the electron density and transfer of part of the iron and molybdenum cations to another valence state:

$\text{Fe}^{3+} + \text{e}^- \rightarrow \text{Fe}^{2+}$ ,  $\text{Mo}^{5+} \rightarrow \text{Mo}^{6+} + \text{e}^-$  and  $\text{Mo}^{5+} \rightarrow \text{Mo}^{4+} - \text{e}^-$  [31–34]. The association of point defects with increasing  $\delta$  has also been found by other researchers [23].

Mössbauer spectroscopy data indicate the possibility of forming associates with the participation of oxygen vacancies. We obtained samples with different oxygen contents by annealing  $\text{Sr}_2\text{FeMoO}_{6-\delta}$  at 1420 K in a stream of the gas mixture 5% $\text{H}_2/\text{Ar}$ : for 20 hours – sample *A-1* ( $\text{Sr}_2\text{FeMoO}_{5.97}$ ,  $P = 76\%$ ), for 50 hours – *A-2* ( $\text{Sr}_2\text{FeMoO}_{5.94}$ ,  $P = 86\%$ ), and for 90 hours – *A-3* ( $\text{Sr}_2\text{FeMoO}_{5.94}$ ,  $P = 93\%$ ).

It has been found that the observed Mössbauer spectra of samples *A-1*, *A-2*, and *A-3* can be decomposed into four magnetic subspectra – sextets S1, S2, S3, and S4 (**Figure 4**). The main parameters of such sextets – the isomer shift ( $\delta_{\text{IS}}$ ) and the hyperfine magnetic field ( $B_{\text{hf}}$ ) presented in **Table 1** – correspond to the structure of the  $\text{Sr}_2\text{FeMoO}_{6-\delta}$  compound.

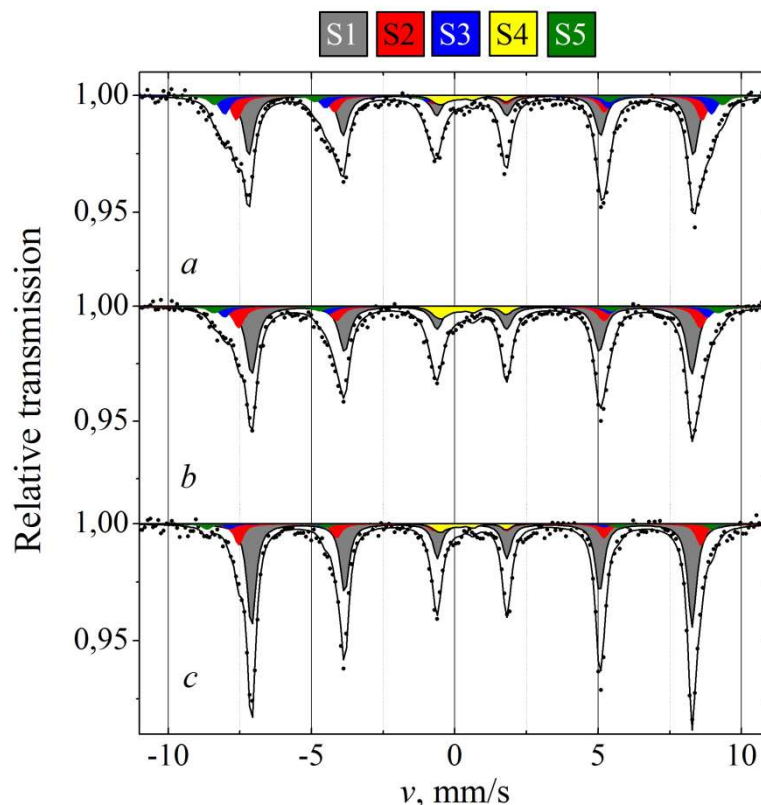


**Figure 4** (color online). Mössbauer spectra of samples *A-1* (*a*), *A-2* (*b*), *A-3* (*c*) obtained at 10 K (gray sextet – S1, red sextet – S2, blue sextet – S3, yellow sextet – S4, green sextet – S5).

The most intense sextet S1, which has the largest relative contribution for sample *A*–3 in comparison to other samples, occupies 60–66% of the total peak area. It indicates the presence of iron cations in the crystallographic positions of an ordered double perovskite. This circumstance indicates the presence of regions with ordered Fe/Mo cations that occupy a larger volume in *A*–3 than in *A*–1 or *A*–2. According to the Mössbauer spectroscopy data, the  $B_{\text{hf}}$  and  $\delta_{\text{IS}}$  values for the S1 sextet (and to a lesser extent for the S2 and S3 sextets) are shifted from the values characteristic of  $\text{Fe}^{3+}$  and correspond to the state with a mixed valence of iron cations  $\text{Fe}^{2+/3+}$  (between  $\text{Fe}^{3+}$  and  $\text{Fe}^{2+}$  [20,35–37]). Thus, the isomeric shift of the S1 sextet for samples *A*–1, *A*–2 and *A*–3 is  $\delta_{\text{IS}} \approx 0.7$  mm/s, which is a value intermediate between those for  $\text{Fe}^{3+}$  ( $\delta_{\text{IS}} \approx 0.5$  mm/s) and  $\text{Fe}^{2+}$  ( $\delta_{\text{IS}} \approx 1.2$  mm/s), as previously found for  $\text{Sr}_2\text{FeWO}_6$  [38,39]. At the same time, the magnitude of the hyperfine magnetic field  $B_{\text{hf}} \approx 47.6$  T is lower than expected for  $\text{Fe}^{3+}$  ( $B_{\text{hf}} \approx 52.3$  T), but higher than for  $\text{Fe}^{2+}$  ( $B_{\text{hf}} \approx 43.2$  T), which also indicates a mixed valence state of iron cations. Since the S1 sextet belongs to Fe cations that are in a perfect superstructural ordering with Mo cations, it cannot be associated with defects in the SFMO structure.

**Table 1.** Hyperfine interaction parameters obtained from the fitting of the Mössbauer spectra of samples *A*–1, *A*–2, and *A*–3 measured at 10 K with sextets of Gaussian components S1 – S5:  $\delta_{\text{IS}}$  (mm/s) is the isomeric shift;  $B_{\text{hf}}$  (T) is the hyperfine magnetic field;  $\Gamma$  (mm/s) is the line width,  $2\varepsilon$  (mm/s) is the quadrupole shift, and  $A$  (%) is the relative contribution.

Sample	Sextett	$A$ , %	$\Gamma$ , mm/s	$2\varepsilon$ , mm/s	$B$ , T	$\delta_{\text{IS}}$ , mm/s
<i>A</i> –1 $\delta=0.03$ $P=76\%$	S1	60±3	0.46±0.01	0.01±0.01	47.61±0.03	0.698±0.003
	S2	13±2	0.31±0.05	0.05±0.02	49.63±0.08	0.631±0.009
	S3	6±3	0.3±0.1	0.09±0.04	51.4±0.2	0.553±0.019
	S4	13±3	0.56±0.09	–0.1±0.04	53.6±0.3	0.53±0.02
	S5	8±1	0.6±0.2	1.12±0.09	7.7±0.2	0.36±0.04
<i>A</i> –2 $\delta=0.06$ $P=86\%$	S1	66±3	0.35±0.01	0.01±0.01	47.60±0.02	0.705±0.002
	S2	10±3	0.23±0.05	0.05±0.02	49.12±0.07	0.674±0.008
	S3	10±2	0.33±0.07	0.09±0.03	50.84±0.13	0.594±0.013

	S4	9±3	0.9±0.3	0.02±0.12	55.8±0.5	0.52±0.06
	S5	5±1	0.5±0.1	0.7±0.1	7.9±0.2	0.51±0.04
<i>A-3</i> $\delta=0.06$ $P=93\%$	S1	68±3	0.35±0.01	0.01±0.01	47.58±0.02	0.71±0.002
	S2	11±3	0.23±0.05	0.05±0.02	49.12±0.07	0.674±0.008
	S3	11±3	0.33±0.07	0.09±0.03	50.84±0.13	0.594±0.013
	S4	6±2	0.9±0.3	0.02±0.12	55.8±0.5	0.52±0.06
	S5	3±2	0.5±0.1	0.7±0.1	7.9±0.2	0.51±0.04

In this case, the mixed valence state of iron cations, associated with the S1 sextet, is mainly due to the presence of a delocalized Mo electron near the Fe atom<sup>[35–37]</sup>. According to calculations of the electronic structure<sup>[14]</sup>, an overlap of the  $4d^1\{S=1/2\}$  level of Mo and the low-spin  $4d^0\{S=0\}$  level of Fe occurs in SFMO. The overlap leads to a shift of the Mo- $4d^1$  electron to the iron position, as a result of which the valence of  $\text{Fe}^{3+}$  decreases to the mixed  $\text{Fe}^{2+/3+}$  state<sup>[20,35–37]</sup>. Compared to other samples, *A-3* has the highest relative contribution of the main sextet S1, which is associated with the lowest Fe valence, that is, the maximum achievable density of a delocalized electron at the Fe positions, in the case of an ordered state of Fe/Mo cations.

The less intense sextets S2 and S3, constituting 19 – 20% of the relative contribution, with a smaller isomeric shift and larger  $B_{\text{hf}}$  values, correspond to iron cations surrounded by antisite defects, oxygen vacancies and their associates. The S2 and S3 sextets, whose lines overlap with S1, represent a state of iron where the density of delocalized electrons is lower than in S1, due to the influence of defects. As can be seen in Table 1, an increase in  $\delta$  leads to an increase in the relative contribution of the S1 component in the Mössbauer spectra of sample *A-3*, corresponding, as mentioned earlier, to iron ions in the mixed valence state  $\text{Fe}^{2+/3+}$ . In this case, a decrease in the relative contribution of the S2 component is observed, which indicates an increase in the structural ordering due to a decrease in the concentrations of the antisite defects,  $[\text{Fe}_{\text{Mo}}]$  and  $[\text{Mo}_{\text{Fe}}]$ , as well as a possible rearrangement of anion vacancies with the formation of their associates. At the same time,

an increase in the oxygen deficiency index  $\delta$  increases the number of oxygen vacancies and can lead to a disruption of the order in the structure. However, the oxygen deficiency in the samples is relatively small, and for  $\delta = 0.04$ , the concentration of oxygen vacancies is  $[V_0] \sim 0.7\%/f.u.$ , which cannot provoke a distortion of the double perovskite structural symmetry. Consequently, an increase in the intensity of S1 with a decrease in S3 and S4 may be more related to the superstructural ordering of Fe/Mo cations. The ordering is facilitated by an increased number of oxygen defects. This means that the presence of anionic vacancies in the double perovskite structure contributes to the diffusion mobility of iron and molybdenum cations and, accordingly, to the enhancement of the long-chain ordering of Fe/Mo. Thus, the delocalized electron density on the Fe cation, which determines the change in the isomer shift, depends primarily on the presence of antisite defects.

An increase in the intensity of S3, as well as a decrease in the intensities of S4 and S5, can be associated with changes in the distribution of electrons and with a redistribution of defects at a greater oxygen deficiency. Moreover, changes in the quadrupole shift of S3 and S4 indicate a modification of the local symmetry of the environment of iron cations. So, the quadrupole displacement  $2\varepsilon \approx 0$  mm/s for the S1 sextet agrees well with the cubic local symmetry, while the deviation from  $2\varepsilon \approx 0$  mm/s for sextets S2, S3 and S4 in the range  $2\varepsilon \approx (-0.05 \dots -0.1)$  mm/s indicates a change in the local symmetry from cubic to tetrahedral. A significant increase in the isomer shift for sextets S2 and S3 (Table 1) for sample A-3 is consistent with a redistribution of the electron density with increasing oxygen deficiency. It has been found that with increasing nonstoichiometry index  $\delta$ , a shift is observed in the values of  $\delta_{IS}$  and  $B_{hf}$  toward the divalent state of iron cations, which suggests that the lower symmetry in the distribution of the electron density on Fe cations leads to a decrease in the isomeric shift.

However, the effect of electron density redistribution is greater than the effect of the presence of point defects, since it can affect Fe cations at a longer distance than anion vacancies, their associates, and other defects. An increase in the concentration of antisite defects contributes to a decrease in the delocalized Mo electron density on neighboring Fe sites. The strongest effect of

anionic vacancies can be associated with the S4 sextet, whose parameters are close (within the experimental error) to those of the  $\text{Fe}^{3+}$  ions ( $\delta_{\text{IS}} \approx 0.5$  mm/s,  $B_{\text{hf}} \approx 55$  T, as, e.g., in hematite<sup>[40]</sup>). Therefore, a change in the isomer shift  $\Delta\delta_{\text{IS}} = 0.2$  mm/s can be explained by a decrease in the number of delocalized electrons. The intensity of the S4 sextet decreases with increasing oxygen nonstoichiometry, which is due to the formation of oxygen vacancies associates. This conclusion is justified by the fact that the appearance of oxygen vacancies and their ordering contribute to obtaining such values of the isomer shift of the Mössbauer spectral components when some of the iron ions occupy positions in a tetrahedral or similar environment, which indicates the formation of associates of oxygen vacancies.

An increase in the annealing time up to 90 hours in a stream of 5% $\text{H}_2/\text{Ar}$  at  $T = 1420$  K facilitates the transfer of part of molybdenum cations to another valence state:  $\text{Mo}^{6+} + xe^{-1} \rightarrow \text{Mo}^{5+} + \text{Mo}^{4+} + \text{Mo}^{x+}$  (**Figure 5**). This indicates a redistribution of the electron density stimulated by the formation of oxygen vacancies associates<sup>[20,32]</sup>.

The XPS analysis of the chemical state of molybdenum cations in samples *A-1*, *A-2* and *A-3* has shown that the core level Mo-3*d* is a spin-orbit doublet consisting of two sublevels, Mo-3*d*<sub>5/2</sub> and Mo-3*d*<sub>3/2</sub> (Figures 5 *a*, *c*, *e*). A similar situation was observed for iron ions: the core level Fe-2*p* is a spin-orbit doublet consisting of two sublevels, Fe-2*p*<sub>3/2</sub> and Fe-2*p*<sub>1/2</sub> (Figures 5 *b*, *d*, *f*). To evaluate the valence state of the molybdenum cations, a fitting procedure was performed using the 3.13 eV spin-orbit doublet splitting and the (Mo-3*d*<sub>5/2</sub>):(Mo-3*d*<sub>3/2</sub>) area ratio was fixed to be equal to 3:2<sup>[41]</sup>. In the case of the valence state of iron cations, a fitting was performed using the 13.6 eV spin-orbit doublet splitting while the ratio of the peaks was set to 2:1<sup>[41]</sup>.

A deconvolution of the photoelectron emission spectra in the Fe-2*p* region for samples *A-1*, *A-2* and *A-3* showed that the Fe-2*p* spectrum is a superposition of four components – two for Fe-2*p*<sub>3/2</sub> and two for Fe-2*p*<sub>1/2</sub> (Figures 5 *b*, *d*, *e*). It indicates the presence of a  $\text{Fe}^{2+}/\text{Fe}^{3+}$  mixed valence state. The binding energy values of the fitted peaks (**Table 2**) for all samples are in a good agreement with the Fe-2*p*<sub>3/2</sub> positions reported in the literature<sup>[21,42,43]</sup>.

A deconvolution of the photoelectron emission spectra in the Mo-3d region for samples *A-1* and *A-2* (Figures 5 *a, c*) showed that the Mo-3d spectrum is a superposition of four components – two for Mo-3d<sub>3/2</sub> and two for Mo-3d<sub>5/2</sub> – indicating the presence of a Mo<sup>5+</sup>/Mo<sup>6+</sup> mixed valence state.

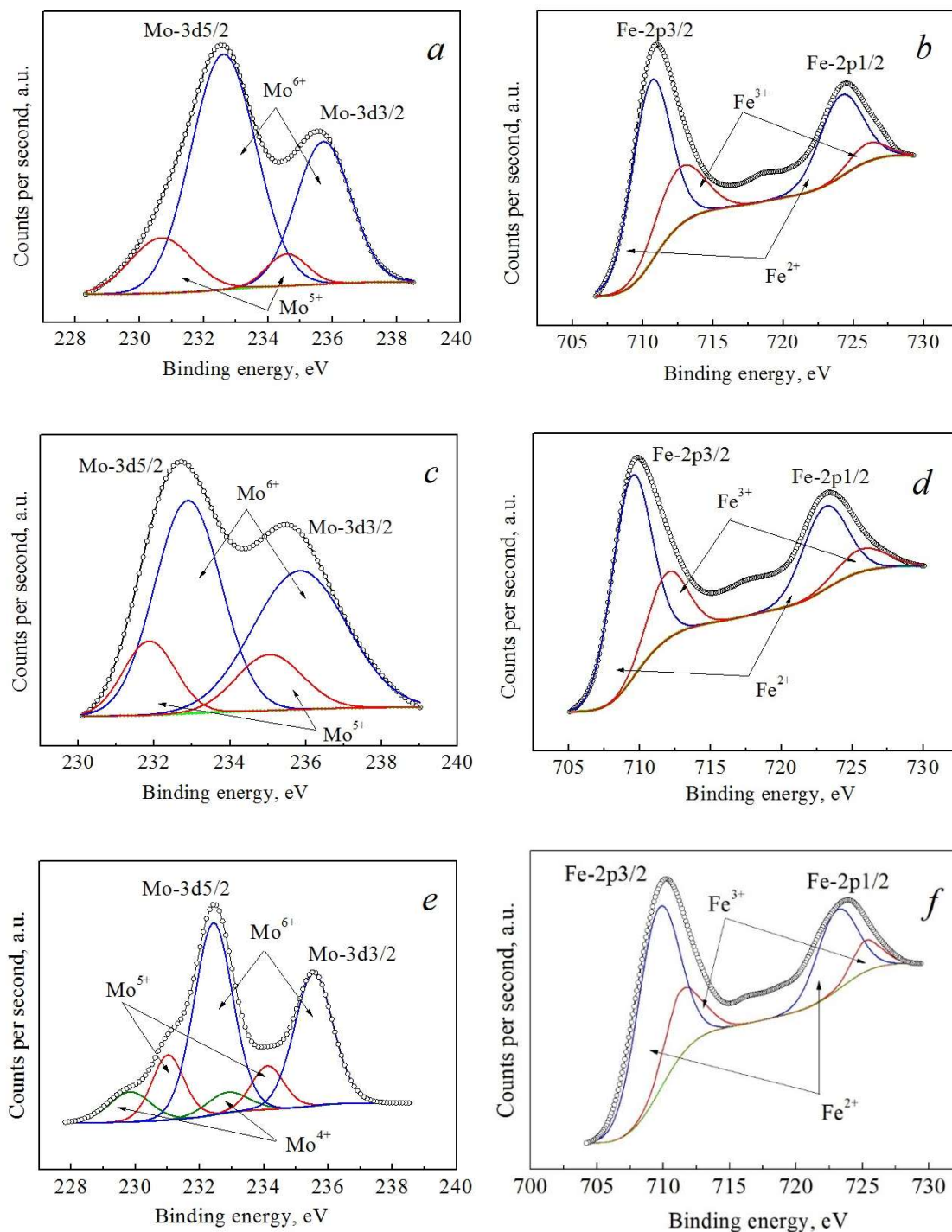


**Figure 5** (color online). XPS spectra of the core levels of Mo-3d (*a, c, e*) and Fe-2p (*b, d, f*) of *A-1* (*a, b*), *A-2* (*c, d*), *A-3* (*e, f*) samples.

For sample *A-3*, the Mo-3*d* regions were fitted using six peaks indicating the presence of a mixed valence state of Mo<sup>4+</sup>, Mo<sup>5+</sup>, Mo<sup>6+</sup> (Figure 5 *e*). The binding energy values of all fitted peaks (Table 2) are in a good agreement with the reported Mo-3*d*<sub>5/2</sub> positions [21,42,43]: 229.6 eV, 230.7 eV and 232.4 eV for the Mo<sup>4+</sup>, Mo<sup>5+</sup> and Mo<sup>6+</sup> valence states, respectively.

It should be noted that the spectral features of Mo<sup>5+</sup> with increasing binding energy and the increase of the Mo<sup>4+</sup> concentration correspond to an increase in the superstructural ordering of Fe/Mo cations (Table 2). In contrast to the increase in *P*, the binding energy of the Mo<sup>6+</sup> cations and their concentration decrease.

**Table 2.** Binding energy (BE) of the Mo-3*d*<sub>5/2</sub> and Fe-2*p*<sub>3/2</sub> core electron levels and the percentage ratio of the valence states of Mo/Fe cations in the SFMO compound.

Sample	<i>BE</i> (Mo-3 <i>d</i> <sub>5/2</sub> ), eV			<i>BE</i> (Fe-2 <i>p</i> <sub>3/2</sub> ), eV	
	Mo <sup>6+</sup>	Mo <sup>5+</sup>	Mo <sup>4+</sup>	Fe <sup>2+</sup>	Fe <sup>3+</sup>
<i>A-1</i>	232.61 (84%)	230.67 (16%)	–	710.57 (81%)	712.63 (19%)
<i>A-2</i>	232.74 (79%)	232.11 (21%)	–	709.43 (74%)	711.96 (26%)
<i>A-3</i>	232.39 (68%)	231.01 (20%)	229.70 (12%)	709.58 (71%)	711.61 (29%)

The XPS results show that the increase of the superstructural ordering in SFMO causes the appearance of molybdenum cations in new valence states. With increasing annealing time at *T* = 1420 K in a stream of 5%*H*<sub>2</sub>/*Ar* for *t* = 90 h, the Mo<sup>6+</sup> and Fe<sup>2+</sup> concentrations decrease (Figure 5). At the same time, due to the redistribution of the electron density, the number of Mo<sup>5+</sup> and Fe<sup>3+</sup> cations increases, and molybdenum cations with a Mo<sup>4+</sup> valence appear.

### 3. Conclusions

Basing on the temperature dependences of the oxygen desorption dynamics in Sr<sub>2</sub>FeMoO<sub>6-δ</sub>, the activation energy of oxygen diffusion was determined by the Merzhanov technique. It has been established that at the initial stage of the oxygen desorption the activation energy has a minimal

value of 76.7 kJ/mol at the oxygen deficiency index  $\delta = 0.005$ . As the concentration of oxygen vacancies increases, the activation energy rises to 156.3 kJ/mol at  $\delta = 0.06$ . This fact indicates the appearance of forces which prevent the diffusion of oxygen during its desorption. It is assumed that as  $\delta$  grows, the mechanism of defect formation changes, affecting the anions' mobility. It is quite possible that, with an increase in the concentration of oxygen vacancies, an interaction occurs between them and the nearest cations, with the subsequent formation of associates of various types that are less mobile than single anion vacancies.

According to the data of Mössbauer spectroscopy, it has been established that an increase in the concentration of oxygen vacancies leads to an increase in the isomer shift  $\delta_{\text{IS}}$  up to 0.7 mm/s and to the formation of an intermediate ( $\text{Fe}^{2+/3+}$ ) valence state of iron, which is promoted by the formation of associates of anionic vacancies. In this case, the appearance of oxygen vacancies and their ordering lead to a situation in which some of the iron ions occupy positions in a tetrahedral (or close to it) environment.

The XPS results show that the increase in the oxygen vacancies concentration results in decreasing  $\text{Mo}^{6+}$  and  $\text{Fe}^{2+}$  concentrations. At the same time, due to the redistribution of the electron density, the number of  $\text{Mo}^{5+}$  and  $\text{Fe}^{3+}$  cations increases, and molybdenum cations in a different charge state ( $\text{Mo}^{4+}$ ) appear, which indirectly indicates the presence of associates of oxygen vacancies.

### **Acknowledgements**

The work has been supported by the European Project H2020 – MSCA – RISE – 2017 – 778308 – SPINMULTIFILM. N.A.S. gratefully acknowledges the financial support by the FCT of Portugal through the Project No. I3N/ FSCOSD (Ref. FCT UID/CTM/50025/2019) and by the Ministry of Education and Science of the Russian Federation in the framework of the Increase Competitiveness Program of NUST «MISiS» (no. K2-2019-015).

## References

- [1] D. Serrate, J.M. De Teresa, M.R. Ibarra, *J. Phys. Condens. Matter* **2007**, *19*, 1.
- [2] D. Topwal, D.D. Sarma, H. Kato, Y. Tokura, M. Avignon, *Phys. Rev. B* **2006**, *73*, 0944191.
- [3] T.S. Chana, R.S. Liua, S.F. Hub, J.G. Linc, *Mater. Chem. Phys.* **2005**, *93*, 314.
- [4] L.V. Kovalev, M.V. Yarmolich, M.L. Petrova, J. Ustarroz, H. Terryn, N.A. Kalanda, M.L. Zheludkevich, *ACS Appl. Mater. Interfaces* **2014**, *6*, 19201.
- [5] L. dos Santos–Gómez, L. León–Reina, J.M. Porrás–Vázquez, E.R. Losilla, *Solid State Ion.* **2013**, *239*, 1.
- [6] N. Kalanda, D.–H. Kim, S. Demyanov, S.–C. Yu, M. Yarmolich, A. Petrov, S.K. Oh, *Curr. Appl. Phys.* **2018**, *18*, 27.
- [7] D. Stoeffler, S. Colis, *J. Phys. Condens. Matter* **2005**, *17*, 6415.
- [8] M.V. Yarmolich, N.A. Kalanda, A.A. Yaremchenko, S.A. Gavrilov, A.A. Dronov, M.V. Silibin, *Inorg. Mater.* **2017**, *53*, 70.
- [9] J. Rager, M. Zipperle, A. Sharma, J.L. MacManus–Driscoll, *J. Am. Ceram. Soc.* **2004**, *87*, 1330.
- [10] F. Liscio, F. Bardelli, C. Meneghini, S. Mobilio, S. Ray, D.D. Sarma, *Nucl. Instr. Meth. Phys. Res. B* **2006**, *246*, 189.
- [11] R. Allub, O. Navarro, M. Avignon, B. Alascio, *Physica B Condens Matter.* **2002**, *320*, 13.
- [12] M. Tovar, M.T. Causa, A. Butera, J. Navarro, B. Martínez, J. Fontcuberta, M.C.G. Passeggi, *Phys. Rev. B* **2002**, *66*, 024409.
- [13] J. Lindén, T. Yamamoto, M. Karppinen, H. Yamauchi, *Appl. Phys. Lett.* **2000**, *76*, 2925.
- [14] D.D. Sarma, P. Mahadevan, S. Ray, A. Kumar, *Phys. Rev. Lett.* **2000**, *85*, 2549.
- [15] D. Niebieskikwiat, A. Caneiro, R.D. Sánchez, J. Fontcuberta, *Phys. Rev. B* **2001**, *64*, 180406.
- [16] B. Jurca, J. Berthon, N. Dragoe, P. Berthet, *J. Alloys Comp.* **2009**, *474*, 416.
- [17] J. MacManus–Driscoll, A. Sharma, Y. Bugoslavsky, W. Branford, L.F. Cohen, M. Wei, *Adv. Mater.* **2006**, *18*, 900.
- [18] Y. Matsuda, M. Karppinen, Y. Yamazaki, H. Yamauchi, *J. Solid State Chem.* **2019**, *182*, 1713.
- [19] A. Sharma, J.L. MacManus–Driscoll, W. Branford, Y. Bugoslavsky, L.F. Cohen, J. Rager, *Appl. Phys. Lett.* **2005**, *87*, 112505.
- [20] M. Yarmolich, N. Kalanda, S. Demyanov, Ju. Fedotova, V. Bayev, N.A. Sobolev, *Phys. Status Solidi B* **2016**, *253*, 2160.
- [21] M. Raekers, K. Kuepper, H. Hesse, I. Balasz, I.G. Deac, S. Constantinescu, E. Burzo, M. Valeanu, M. Neumann, *J. Optoelectron. Adv. M.* **2006**, *8*, 455.
- [22] J. Santiso, A. Figueras, J. Fraxedas, *Surf. Interface Anal.* **2002**, *33*, 676.
- [23] Yi-Long Chen, De-Ping Yang, *Mössbauer Effect in Lattice Dynamics: Experimental Techniques and Applications*, Wiley-VCH Verlag GmbH & Co. KGaA, Weinheim **2007**.
- [24] Z. Klencsár, Z. Németh, A. Vértes, I. Kotsis, M. Nagy, Á. Cziráki, C. Ulhaq–Bouillet, V. Pierron–Bohnes, K. Vad, S. Mészáros, J. Hakl, *J. Magn. Magn. Mater.* **2004**, *281*, 115.
- [25] O. Chmaissem, R. Kruk, B. Dabrowski, D.E. Brown, X. Xiong, S. Kolesnik, J. D. Jorgensen, C.W. Kimball, *Phys. Rev. B* **2000**, *62*, 14197.
- [26] W. Kraus, *J. Appl. Crystallogr.* **1996**, *29*, 301.
- [27] J. Rodríguez–Carvajal, *Newsletter* **2001**, *26*, 12.
- [28] N.A. Kalanda, *Mod. Electron. Mater.* **2018**, *4*, 1.
- [29] A.G. Merzhanov, V.V. Barzykin, A.S. Shteinberg, V.T. Gontkovskaya, *Thermochimica Acta* **1977**, *21*, 301.
- [30] D. Sánchez–Rodríguez, H. Eloussifi, J. Farjas, P. Roura, M. Dammak, *Thermochimica Acta* **2014**, *589*, 37.

- [31] R. Kircheisen, J. Topfer, *J. Solid State Chem.* **2012**, 185, 76.
- [32] N. Kalanda, V. Turchenko, D. Karpinsky, S. Demyanov, M. Yarmolich, M. Balasoiu, N. Lupu, S. Tyutyunnikov, N.A. Sobolev, *Phys. Status Solidi B* **2019**, 256, 1800278.
- [33] H. Kawanaka, I. Hase, S. Toyama, Y. Nishihara, *J. Phys. Soc. Jpn.* **1999**, 68, 2890.
- [34] T. Suominen, J. Raittila, T. Salminen, K. Schlesier, J. Lindén, P. Paturi, *J. Magn. Magn. Mater.* **2007**, 309, 278.
- [35] J.M. Greneche, M. Venkatesan, R. Suryanarayanan, J.M.D. Coey, *Phys. Rev. B* **2001**, 63, 174403.
- [36] M. Venkatesan, M. Grafoute, A.P. Douvalis, J.M. Greneche, R. Suryanarayanan, J.M.D. Coey, *J. Magn. Magn. Mater.* **2002**, 242, 744.
- [37] K. Kuepper, I. Balasz, H. Hesse, A. Winiarski, K.C. Prince, M. Matteucci, D. Wett, R. Szargan, E. Burzo, M. Neumann, *Phys. Status Solidi A* **2004**, 201, 3252.
- [38] H. Kawanaka, I. Hase, S. Toyama, Y. Nishihara, *Physica B Condens. Matter.* **2000**, 281, 518.
- [39] A.P. Douvalis, M. Venkatesan, J.M.D. Coey, M. Grafoute, J.-M. Greneche, R. Suryanarayanan, *J. Phys. Condens. Matter* **2002**, 14, 12611.
- [40] J. Jacob, M. Abdul Khadar, *J. Magn. Magn. Mater.* **2010**, 332, 614.
- [41] C.D. Wagner, W.M. Riggs, L.E. Davis, J.F. Moulder, *Handbook of X-ray Photoelectron Spectroscopy: A Reference Book of Standard Data for Use in X-ray Photoelectron Spectroscopy*, edited by G.E. Muilenberg, Physical Electronics Division, Perkin-Elmer Corp., Eden Prairie, MN, **1979**.
- [42] K. Kuepper, I. Balasz, H. Hesse, A. Winiarski, K.C. Prince, M. Matteucci, D. Wett, R. Szargan, E. Burzo, M. Neumann, *Phys. Status Solidi A* **2004**, 201, 3252.
- [43] M. Retuerto, F. Jimenez-Villacorta, M.J. Martinez-Lope, Y. Huttel, E. Roman, M.T. Fernandez-Díaz, J.A. Alonso, *Phys. Chem. Chem. Phys.* **2010**, 12, 13616.